CrystEngComm

Direct observation of monoclinic ferroelectric phase and domain switching process in Sodium-Potassium Niobate single crystals

Journal:	*CrystEngComm*
Manuscript ID:	CE-ART-11-2014-002199.R3
Article Type:	Paper
Date Submitted by the Author:	26-Feb-2015

Complete List of Authors:	Deng, Hao; Shanghai Institute of Ceramics, University of Chinese Academy of Sciences, Key Laboratory of Inorganic Functional Materials and Devices Zhang, Haiwu; Shanghai Institute of Ceramics, University of Chinese Academy of Sciences, Key Laboratory of Inorganic Functional Materials and Devices Shanghai Zhao, Xiangyong; Shanghai Institute of Ceramics, University of Chinese Academy of Sciences, Key Laboratory of Inorganic Functional Materials and Devices Shanghai Chen, Chao; Shanghai Institute of Ceramics, University of Chinese Academy of Sciences, Key Laboratory of Inorganic Functional Materials and Devices Shanghai Wang, Xi'an; Shanghai Institute of Ceramics, University of Chinese Academy of Sciences, Key Laboratory of Inorganic Functional Materials and Devices Shanghai Li, Xiaobing; Shanghai Institute of Ceramics, University of Chinese Academy of Sciences, Key Laboratory of Inorganic Functional Materials and Devices Shanghai Lin, Di; Shanghai Institute of Ceramics, University of Chinese Academy of Sciences, Key Laboratory of Inorganic Functional Materials and Devices Shanghai Ren, Bo; Shanghai Institute of Ceramics, University of Chinese Academy of Sciences, Key Laboratory of Inorganic Functional Materials and Devices Shanghai Jiao, Jie; Shanghai Institute of Ceramics, University of Chinese Academy of Sciences, Key Laboratory of Inorganic Functional Materials and Devices Shanghai Luo, Haosu; Shanghai Institute of Ceramics, University of Chinese Academy of Sciences, Key Laboratory of Inorganic Functional Materials and Devices Shanghai, China

Direct observation of monoclinic ferroelectric phase and domain switching process in $(K_{0.25}Na_{0.75})NbO_3$ single crystals

Hao Deng[1,2] Haiwu Zhang[1,2] , Xiangyong Zhao[1] ,Chao Chen[1, 2], Xi'an Wang[1], Xiaobing Li[1], Di Lin[1], Bo Ren[1], Jie Jiao[1], Haosu Luo[1 a)]

[1]Key Laboratory of Inorganic Functional Materials and Devices, Shanghai Institute of Ceramics, University of Chinese Academy of Sciences, 215 Chengbei Road, Jiading, Shanghai 201800, China

[2] University of Chinese Academy of Sciences, Beijing, 001049, China

Abstract

In situ observations of the phase symmetry and domain evolution of $(K_{0.25}Na_{0.75})NbO_3$ single crystals under bipolar electric fields have been performed for both pseudocubic (110) and (001) orientations using polarized light microscopy and X-ray Diffraction. The macroscopic symmetry was identified to be monoclinic C type phase with the spontaneous polarization direction close to <054>. The electric field driven domain-morphology and evolution model were also presented. It was found that, under antiparallel electric field, the approximate 180° domain switching process in pseudocubic (101) sample consists of three steps: two ~60° domain switching and a ~90° domain switching, and the ~90° domain switching process in the pseudocubic (001) sample is composed of two ~60°switching steps.

Introduction

Potassium sodium niobate $(K_xNa_{1-x})NbO_3$ based solid solutions (KNN) have attracted remarkable attention in recent years for their great prospective of replacing

[a] hsluo@mail.sic.ac.cn

widely used lead zirconate titanate (PZT) materials, in view of their superior piezoelectric performance[1-5]. However, understanding the nature of KNN，specifically phase and domain switching process，is an extremely tough yet intriguing task. Numerous experiments have been performed on KNN ceramics and powders in 1950~1970s, such as X-ray and neutron diffraction, producing highly complex and often controversial pictures[6-12]. All these studies broadly agree that a nearly composition independent polymorphic phase boundary (PPB) exists around 200℃ and three phase boundaries present at about x=0.18, 0.32 and 0.48 at room temperature. Nevertheless, the crystallographic nature of the KNN with compositions on the side of x<0.5 has been a point of debate. The room temperature crystallographic structure of Na rich KNN was first proposed by Shirane *et al.*as orthorhombic[6], which was incorporated in the classic textbook by Jaffe *et al.*[13]. Later, a number of investigations alternatively suggested the possible space group to be *Pm* (Glazer notation $a^{-}b^{+}c^{0}$) for 0.18<x<0.32[9-12]. The accuracy of these refinements was limited by facility, i.e. the interference of Cu $K_{\alpha 2}$ or even K_{β} and lack of high precision Goniometer and effective detector. Since the breakthrough made by Saito *et al.* in 2004[1], the research on KNN phase diagram have revived interest of crystallographers, which has also been promoted by remarkable technological advancement， i.e. more powerful computer-controlled high-resolution X-ray (HR-XRD) or neutron diffraction and more effective Rietveld refinement. Baker *et al.* refined the room-temperature phase of KNN (0.18<x<0.52) to be *Pm* ($a_{+}^{0}b_{0}^{+}c_{+}^{0}$ for 0.18<x<0.32 and $a_{+}^{0}b_{0}^{0}c_{+}^{0}$ 0.32<x<0.52) [14-16]. Meanwhile, many researchers used the

orthorhombic symmetry for the refinement of the cell parameters of KNN at room temperature from XRD data[17, 18] due to the minor difference between the orthorhombic and monoclinic phases.

The presence of grain boundaries in ceramics and skin effect in powders makes it difficult to determine the macroscopic physical properties, on the other hand, the crystal symmetry may also depend on the length scale under observation[19]. The macroscopic symmetry, which determines the crystal physical properties, can only be precisely established on the basis of high-quality single crystals with size large enough for an optical study. However, growth of KNN crystals with large size and high quality was a challenge. In recent research, Gupta *et al.* [20] reported an optical birefringence study of $(K_xNa_{1-x})NbO_3$ (x=0.4, 0.5 and 0.6) single crystals in the temperature range of 30–600°C and inferred x=0.4 crystals to be a monoclinic C type (M_C, space group *Pm*) structure while x=0.5 crystals to be a monoclinic A or B type (M_A/M_B space group *Cm*) structure. At the same time, a polarized Raman analysis of $(K_{0.5}Na_{0.5})NbO_3$ single crystals presented by Rafiq *et al.* [21] assigned the crystal to the monoclinic *Pm* symmetry. The contradiction may be caused by the low angular resolution of these two methods (orientation distribution plots' accuracy is lower than 5°). Polarizing light microscopy (PLM) is an effective way to investigate the macroscopic symmetry and domain structures[19, 22-25]. In the early PLM work by Lin *et al.* [26] only the O phase was observed probably because of the opaque sample and, more importantly, the lack of data on other orientations than pseudocubic (001) (abbreviated as $(001)_{pc}$). The domain morphology along other orientation, which is of particular importance in

determining the symmetry, and *in situ* domain evolution driven by electric field are seriously deficient, especially based on high quality crystals. The domain structures of KNN are rather intricate and more systematic studies are urgently desired to better understand the structure and motion of domains under electric fields.

In our recent work, large-sized $(K_{0.25}Na_{0.75})NbO_3$ (KNN25) single crystals with high quality and overall performance (d_{33}~145pC/N, k_t~69%) were grown by top seeded solution growth technique (TSSG)[27] and $(101)_{pc}$ orientated crystals were first obtained. We proposed domain switching model to illustrate why the strain of $(110)_{pc}$ orientation is twice that of $(100)_{pc}$. In this work, *in situ* observations of the domain structure evolution under electric field were carried out on both $(101)_{pc}$ and $(001)_{pc}$ KNN25 single crystals by PLM and HR-XRD. The macroscopic structure of KNN25 was identified to be M_C phase, and domain evolution model with *in situ* electric field was established simultaneously, which is almost consistent with our previous hypothesis.

Experimental

KNN25 single crystals with dimension up to Ø30×10mm^3 were grown by carefully controlled TSSG technique[27]. The composition of the specimens was verified using X-ray fluorescence analysis (XRF).The single crystals were sliced into wafers perpendicular to their pseudocubic $[001]_{pc}$ and $[101]_{pc}$ directions and polished with Ø0.5μm diamond lapping pastes to thicknesses of about 40μm. To release residual stress, the crystals were annealed in air at 500°C for 20 hours and then slowly cooled to room temperature at the rate of 0.5°C/min. Half transparent conductive gold electrode

was sputtered on sample surfaces. The thickness of the gold electrode was around 15nm as measured by a Filmetrics F20 spectral refractance thin film analyzer. Then a DC external electric field was applied to the samples by a high voltage amplifier. The domain-switching processes were *in situ* observed by using an Olympus BX51 polarized microscope with a 0°/90° crossed polarizer/analyzer pair. The experimental configuration for observation of domain structure is illustrated in Fig. 1. Then the domain-switching processes were further evidenced by X-ray diffraction using Bruker D8 Discover HRXRD system.

Results and discussion

Generally, a spontaneous polarization (P_S) can be induced in the paraelectric perovskite cubic structure $Pm\bar{3}m$ while cooled below Curie temperature resulting in tetragonal *P4mm* (with P_S along $<001>_{pc}$), rhombohedral *R3m* (P_S along $<111>_{pc}$), orthorhombic *O*(*Amm2*, P_S along $<110>_{pc}$), monoclinic *Pm*(*Mc*, P_S in $\{001\}_{pc}$ plane), two types of monoclinic *Cm*(M_A and M_B with P_S in $\{110\}_{pc}$ plane) or triclinic symmetry, as depicted in Fig. 2(a). According to the Neumann's principle[28], the symmetry of any physical property of a crystal must include the symmetry elements of the point group of the crystal. Orientations of the P_S and their corresponding phases could be revealed by using relations of crystallographic symmetry and optical extinction under polarizing microscopy.

In transparent materials, the refractive index of the medium is anisotropic and the surface of rotation can be represented by an ellipsoid known as the optical indicatrix[28, 29]. For ferroelectric crystals, P_S is along the longest principle axes of the optical

indicatrix. The cross section of refraction index ellipsoid by crystal plate plane would be an ellipse representing the refractive index of perpendicularly transmitted light. Under crossed polarizers, the crystal appears to be in extinction when the major axes of the ellipse (domain's vibration direction or the projection of P_s on the plane) are parallel (or perpendicular) to the polarization directions of the polarizer or analyzer.

The projection of P_s on $(101)_{pc}$ and $(001)_{pc}$ planes were shown in Fig. 2(b) and (c).The principal axes and P_S of T and R phases are along $<001>_{pc}$ and $<111>_{pc}$, respectively. Hence, for the $(001)_{pc}$ plate the vibration direction of all the domains are parallel or perpendicular to each other and the extinction angle θ (defined as the smaller angle between the domain's vibration direction and reference direction-$<\bar{1}01>_{pc}$ for $(101)_{pc}$ samples and $<\bar{1}00>$ for $(001)_{pc}$ samples in this article) is indeed the same for all domains: $\theta = 45°$ in the R phase and $\theta = 0°$ in the T phase. It's worthy to note that extinction in each domain must be automatically observed at $\theta + m90°$ (m is an integer). All these extinction are equivalent and we will only consider angles in the $-45° < \theta < 45°$ range. For the case of $(101)_{pc}$ platelet, the extinction angles in T phase are also $\theta = 0°$; while in R phase extinction may appear at $\theta = 0°$ or at $\theta = \arctan\frac{1}{\sqrt{2}} = 35.3°$.The O phase is optically biaxial: one of the indicatrix axes is parallel to the $<001>_{pc}$ direction and two others are parallel to $<110>_{pc}$, so that different domains may vanish at $\theta = 45°$ or $\theta = 0°$ in the $(001)_{pc}$ platelet, and at $\theta = 0°$ or $\theta = 35.3°$ in $(101)_{pc}$ platelet.

In the optically biaxial M phases, one principal axis is along $<110>_{pc}$ in the *Cm* phases (M_A and M_B) or <001> in the *Pm* (M_C) phase, the polarization and the other two

axes are in the plane perpendicular to that principal axis. For the $(001)_{pc}$ platelet, some domains may extinguish at θ_M, or $-\theta_M$, where $\theta_M \neq 0°/45°$ is a priori unknown and may depend on composition and temperature[19, 30]. The extinction angles of other domains may be $\theta = 45°$ for M_A and M_B phases or $\theta = 0°$ for M_C phase. These two values can be utilized to identify specific Monclinic phase. While for the $(101)_{pc}$ platelet, the extinctions perhaps occur at $\theta = 0°$ in the *Cm* phases or $\theta = 90°$ in the M_C phase[31]. The other possible extinction angles correspond to $\arctan(\frac{1}{\sqrt{2}}\tan\theta_M)$ or $-\arctan(\frac{1}{\sqrt{2}}\tan\theta_M)$ for both *Cm* and M_C phases, and this characteristic angle can also distinguish Monclinic phase from R/T/O phases.

In the following, we show the micrographs of domain patterns during electric field cycling and the corresponding P-E hysteresis loop for both $(101)_{pc}$- and $(001)_{pc}$-oriented single crystals in Figs. 3 and 4, respectively. The P_S states of marked points in P-E loops are also illustrated, which will be discussed later. First, the extinction behaviors were examined. We use P/A to represent the angle between polarizer/analyzer and the reference direction (i. e., $<\bar{1}01>_{pc}$ for $(101)_{pc}$ samples and $<\bar{1}00>$ for $(001)_{pc}$ samples). So when P/A=θ (the extinction angle), extinguish happens. For $(101)_{pc}$ wafer, under positive and negative electric field (Fig. 3(c) and (g)), comparatively large areas appear to be in extinction (black) at $\theta = 29°$ and $\theta = -29°$, respectively. These extinction angles are permissible only in the monoclinic phases. To further confirm the specific symmetry, the domain pattern study of $(001)_{pc}$ wafer is carried out. As clearly seen in Fig. 4(b), when an electric field of 800

V/mm was applied along the $[001]_{pc}$ direction, small extinction area is visible at $\theta = 0°$, which becomes bright at $\theta = 39°$ ($\arctan(\frac{1}{\sqrt{2}}\tan 39°) = 29.8° \approx 29°$). On the other hand, a small bright area (in red circle) for $\theta = 0°$ turns into dark for $\theta = 39°$. The extinction angle $\theta = 0°$, as described above, is not expected for the M_A or M_B structure, leading to the conclusion that our single crystal belongs to the monoclinic M_C phase with *Pm* space-group symmetry and the spontaneous polarization direction is very close to $<054>_{pc}$ ($\tan 39° \approx 0.8 = 4/5$).

Apart from confirming the M_C phase, the complicated domain switching process of KNN25 crystals is also determined. As for the unpoled $(101)_{pc}$ sample (Fig. 3(a)), domains distribute randomly with fine lamella domain walls perpendicular to $[010]_{pc}$, revealing no extinction. When an $[\bar{1}0\bar{1}]_{pc}$ electric field is applied (Fig. 3(b)), the lamella domains remain bright for the crossed polars along $(010)_{pc}$ (i.e. P/A=0°), while dark and light stripes appear alternatively for P/A=29°. This extinction angle corresponds to the polarization vector along $[0\bar{5}4]_{pc}$. The lamella dark areas expanded and merged dramatically with elevated applied field (Fig. 3(c)), that is, the domains along $[0\bar{5}4]_{pc}$ grow. The lateral regions without extinctions may be due to superposed domains with nonparallel vibration directions. When the field reaches 2000V/mm (Fig. 3(d)), lamella domains formed at P/A=0° with occasionally visible extinction areas, probably arising from polarizations rotated to $[\bar{4}0\bar{5}]_{pc}$ direction. Inside each twin, overlapped domains are separated by straight stripes walls forming an angle of about 15° with respect to $[\bar{1}01]_{pc}$. A $[\bar{4}0\bar{5}]_{pc}$ single domain state is expected if the electric field further increases. However, it was not achieved even at 2000V/mm, probably ascribed to the

giant depolarization field. When the electric field decreases to 0 (Fig. 3(e)), an almost single-domain state with P_S along $[\,05\bar{4}\,]_{pc}$ is established. This depolarized phenomenon can be explained in terms of competition between elastic energy and depolarization energy and may account for the low k_t in the $(101)_{pc}$ sample[27]. With negative field applied, almost the same process emerges. Upon the reversal of applied electric field (-600V/mm, Fig. 3(f)), lamella domain walls perpendicular to $[010]_{pc}$ appear again. Adjacent domains exhibit extinction angles of -29° and 29°, indicating that some polarization vectors rotate from $[\,05\bar{4}\,]_{pc}$ to $[054]_{pc}$. For electric field of -1000V/mm (Fig. 3(g)), almost all domains are oriented along $[054]_{pc}$. With the reversed electric field increasing to -2000V/mm (Fig. 3(h)), domains switch to $[405]_{pc}$ and display stripes like the mirror image of the picture of Fig. 3(d). In general, the approximate 180° domain switching process of $(101)_{pc}$-oriented KNN25 single crystal under antiparallel electric field consists of three steps: two ~60°domain switchings (from $[\,\bar{4}05\,]_{pc}$ to $[\,05\bar{4}\,]_{pc}$ and from $[054]_{pc}$ to $[405]_{pc}$) and a ~90° domain switching (from $[\,05\bar{4}\,]_{pc}$ to $[054]_{pc}$).

As for the $(001)_{pc}$ sample, the unpoled state presents polydomain structure. We name the poling vector laying in $(001)_{pc}$ plane ($[\,5\bar{4}0\,]_{pc}$/$[\,\bar{5}\bar{4}0\,]_{pc}$/$[\,450\,]_{pc}$/$[\,\bar{4}\bar{5}0\,]_{pc}$) as domain-1 and others ($[\,0\bar{5}\bar{4}\,]_{pc}$/$[\,05\bar{4}\,]_{pc}$/$[\,\bar{5}0\bar{4}\,]_{pc}$/$[\,50\bar{4}\,]_{pc}$) as domain-2 in $[001]_{pc}$ sample. After an electric field of 800 V/mm was applied along the $[\,00\bar{1}\,]_{pc}$ direction (Fig. 4(b)), there appear extinction areas for both $\theta = 0°$ and $\theta = 39°$, denoting the coexistence of domain-1 and domain-2. Fig. 4(c) shows that the sample has been totally poled by a high external field along the $[\,00\bar{1}\,]_{pc}$ direction, with a single domain

state. Even after the electric field is removed, the whole area remains dark (Fig. 4(d)). In contrast to $(101)_{pc}$ orientation, the low depolarization level in $(001)_{pc}$ should be responsible for the high k_t[27]. During the second half of the electric cycle, similar process repeats. Domain coexistence state were achieved at -800V/mm(Fig. 4(e)), indicating the domain switching process is composed of two-step ~60° domain-switching processes instead of a direct ~90° switching (as hypothesis in ref.27). It's worthy to note that even if extinction angle is 0° in Fig. 4(f), the domain configuration was identified to be a polydomain state for the clear existence of domain wall. The generation of intersecting domain walls instead of parallel ones for $(001)_{pc}$ samples might reasonably explain why their P-E loops are leakier than that of $(101)_{pc}$.

To further confirm the influence of electric field on the domain structure, we performed electric-field-dependent structural investigations by X-ray diffraction (XRD). Different domains may display different diffraction peaks for the sake of different stretch along the crystallographic direction. The variations in intensity of peaks qualitatively reflect the change of relative content of different domains. Fig. 5 displays the changes in the diffraction patterns of $(101)_{pc}$ and $(001)_{pc}$ orientated KNN25 crystals under electric field. As the positive and negative poling processes are similar, we only show the negative process. In $(101)_{pc}$ sample, we define the poling vector close to $[101]_{pc}$ or $[\bar{1}0\bar{1}]_{pc}$ ($[405]_{pc}/[\bar{4}0\bar{5}]_{pc}$ etc.) as domain-1', and others ($[05\bar{4}]_{pc}/[054]_{pc}$ etc.) as domain-2'.There are two diffraction peaks for $(101)_{pc}$ sample in Fig. 5(a), corresponding to the domains-1' and domain-2' reflections of the M_C

phase, respectively. At 0V/mm, the left diffraction peak is pretty lower than the right one, demonstrating the volume fraction domain-1 of is smaller than that of domain-2'. With the increasing electric field, the left (right) diffraction peak grows stronger (weaker) and the left one even overwhelms the right one for the electric field of -2000V/mm. Namely, the applied electric field converts domain-2' to domain-1' effectively. It is worthy to note that, the left peak shifts towards lower angles under electric field, while the right one moves to higher angles, which can be explained within the framework of internal stress of strip domains in the sample. Similarly, in Fig. 5(b), the left and right peaks represent domain-2 and domain-1 in the $(001)_{pc}$ planet, respectively. The domain-2 is more than domain-1 at 0V/mm. Under the electric field of -1000V/mm, the numbers of two domain structures are almost equal. With the electric field further increasing to -2000V/mm, the domain-2 become dominant again. The XRD results in $(110)_{pc}$ and $(100)_{pc}$ consist with PLM study and the domain evolution model was close to our previous hypothesis (ref.27), successfully explained the phenomenon that strain of $(110)_{pc}$ orientation is twice that of $(100)_{pc}$.

In previous domain-switching studies, it was considered that an antiparallel external electric field would change the P_S of the domains to inverse direction and 180° domain switching would not induce internal stress[32]. However, the opposite sign of the converse piezoelectric effects in the switched and unswitched domains would result in internal stress[32]. The internal stress in 180° domain switching was significant and could be effectively relaxed by establishing ~90° and ~60° domains stripes. In the

domain-switching process of $(101)_{pc}$ samples, elastic energy and depolarization energy competed with electrostatic energy generated by the external electric field. Under external electric field, ~90° and ~60° domain switching could nucleate in the positions of the local stress to release elastic energies. For $(001)_{pc}$ samples, ~60° domain switching occurred to release the internal stress in the ~90° domain switching. As the mechanical restriction was relaxed by the formation of ~60° domain, domains switched to the direction of the external field driven by the high electrostatic energy.

Conclusions

In summary, extinction behavior and domain-switching processes for both $(101)_{pc}$ and $(001)_{pc}$ oriented $(K_{0.25}Na_{0.75})NbO_3$ single crystals under an antiparallel electric field were investigated *in situ* by PLM. The macroscopic structure of KNN25 was plausibly verified to be M_C phase with the spontaneous polarization direction close to $<054>_{pc}$. Moreover, it was found that the approximate 180° domain switching process in $(101)_{pc}$ sample consists of three steps: two ~60° domain switching (from $[\bar{4}0\bar{5}]_{pc}$ to $[05\bar{4}]_{pc}$ and from $[054]_{pc}$ to $[405]_{pc}$) and a ~90° domain switching (from $[05\bar{4}]_{pc}$ to $[054]_{pc}$). A single domain state along the electric field direction is very hard to be achieved due to the giant depolarization energy. For the $(001)_{pc}$ sample, the ~90° domain switching process is composed of two-step ~60° domain-switching. The phenomena observed herein will promote the understanding of crystalline structures and polarization reversal in ferroelectrics.

Acknowledgements

This work was financially supported by the Ministry of Science and Technology

of China through 973 Program (No. 2013CB632902), the Natural Science Foundation of China (Nos. 51332009, 51372258, 11304333 and 51272268) and Youth Innovation Promotion Association CAS.

Figure captions

FIG. 1. (Color online) The illustration of the experimental configuration for observing domain structures under the polarizing microscope.

FIG. 2. (Color online) Schematics of (a)P_S directions with respect to cubic unit cell for different FE phases and possible extinction positions of domains in (b) $(101)_{pc}$ and (c) $(001)_{pc}$ crystal plates.

FIG. 3. (Color online) (a)- (h) are micrographs of $(101)_{pc}$ KNN25 crystals at different electric fields as stated. (i) illustrates the corresponding points of (a)-(h) in the hysteresis loop for $(101)_{pc}$ KNN25 crystals. The insets are the schematic configurations of P_S states of the points indicated in the micrograph.

FIG. 4. (Color online) (a)- (f): micrographs of $(001)_{pc}$ KNN25 crystals at different electric fields as stated. (g) illustrates the corresponding points of (a)-(f) in the hysteresis loop for $(001)_{pc}$ KNN25 crystals. The insets are the schematic configurations of P_S states of the points indicated in the micrograph.

FIG. 5. (Color online) XRD patterns of (a) $(101)_{pc}$ and (b) $(001)_{pc}$ KNN25 crystals under electric field

Reference:

1 Y. Saito, H. Takao, T. Tani, T. Nonoyama, K. Takatori, T. Homma, T. Nagaya and M. Nakamura, *Nature*, 2004, **432**, 84-87.

2 Y. P. Guo, K. Kakimoto and H. Ohsato, *Appl. Phys. Lett.*, 2004, **85**, 4121-4123.

3 X. J. Cheng, J. G. Wu, X. P. Wang, B. Y. Zhang, J. G. Zhu, D. Q. Xiao, X. J. Wang and X. J. Lou, *Appl. Phys. Lett.*, 2013, **103**, 052906.

4 X. P. Wang, J. G. Wu, D. Q. Xiao, J. G. Zhu, X. J. Cheng, T. Zheng, B. Y. Zhang, X. J. Lou and X. J. Wang, *J. Am. Chem. Soc.*, 2014, **136**, 2905-2910.

5 B. Y. Zhang, J. G. Wu, X. J. Cheng, X. P. Wang, D. Q. Xiao, J. G. Zhu, X. J. Wang and X. J. Lou, *Acs Applied Materials & Interfaces*, 2013, **5**, 7718-7725.

6 G. Shirane, R. Newnham and R. Pepinsky, *Phys. Rev.*, 1954, **96**, 581-588.

7 A. Reisman and E. Banks, *J. Am. Chem. Soc.*, 1958, **80**, 1877-1882.

8 V. J. Tennery and K. W. Hang, *J. Appl. Phys.*, 1968, **39**, 4749-4753.

9 M. Ahtee and A. M. Glazer, *Acta Crystallogr. A*, 1976, **32**, 434-446.

10 M. Ahtee and A. M. Glazer, *Ferroelectrics*, 1976, **12**, 205-206.

11 M. Ahtee and A. W. Hewat, *Acta Crystallogr. A*, 1975, **31**, 846-850.

12 M. Ahtee and A. M. Glazer, *Ferroelectrics*, 1974, **7**, 93-95.

13 B. Jaffe, W. R. Cook and H. L. Jaffe, *Piezoelectric ceramics*, Academic Press, London, New York,, 1971.

14 D. W. Baker, P. A. Thomas, N. Zhang and A. M. Glazer, *Appl. Phys. Lett.*, 2009, **95**, 091903.

15 D. W. Baker, P. A. Thomas, N. Zhang and A. M. Glazer, *Acta Crystallogr. B*, 2009, **65**, 22-28.

16 N. Zhang, A. M. Glazer, D. Baker and P. A. Thomas, *Acta Crystallogr. B*, 2009, **65**, 291-299.

17 H. E. Mgbemere, R. P. Herber and G. A. Schneider, *J. Eur. Ceram. Soc.*, 2009, **29**, 1729-1733.

18 H. E. Mgbemere, M. Hinterstein and G. A. Schneider, *J. Eur. Ceram. Soc.*, 2012, **32**, 4341-4352.

19 A. A. Bokov, X. F. Long and Z. G. Ye, *Phys. Rev. B*, 2010, **81**, 172103.

20 S. Gupta, S. Huband, D. S. Keeble, D. Walker, P. Thomas, D. Viehland and S. Priya, *CrystEngComm*, 2013, **15**, 6790-6799.

21 M. A. Rafiq, P. Supancic, M. E. Costa, P. M. Vilarinho and M. Deluca, *Appl. Phys. Lett.*, 2014, **104**, 011902.

22 A. A. Bokov and Z. G. Ye, *J. Appl. Phys.*, 2004, **95**, 6347-6359.

23 C. S. Tu, C. L. Tsai, J. S. Chen and V. H. Schmidt, *Phys. Rev. B*, 2002, **65**, 104113.

24 C. S. Tu, V. H. Schmidt, I. C. Shih and R. Chien, *Phys. Rev. B*, 2003, **67**, 020102.

25 W. W. Ge, J. F. Li, D. Viehland and H. S. Luo, *J. Am. Ceram. Soc.*, 2010, **93**, 1372-1377.

26 D. B. Lin, Z. R. Li, S. J. Zhang, Z. Xu and X. Yao, *Solid State Commun.*, 2009, **149**, 1646-1649.

27 H. Deng, X. Y. Zhao, H. W. Zhang, C. Chen, X. B. Li, D. Lin, B. Ren, J. Jiao and H. S. Luo, *CrystEngComm*, 2014, **16**, 2760-2765.

28 R. E. Newnham, *Properties of materials : anisotropy, symmetry, structure*, Oxford University Press, Oxford ; New York, 2005.

29 J. F. Nye, *Physical properties of crystals, their representation by tensors and matrices*, Clarendon Press, Oxford, 1957.

30 F. Fang, X. Luo and W. Yang, *Phys. Rev. B*, 2009, **79**, 174118.

31 R. R. Chien, V. H. Schmidt, C. S. Tu and F. T. Wang, *J. Appl. Phys.*, 2005, **98**, 114106.

32 B. Jiang, Y. Bai, W. Y. Chu, Y. J. Su and L. J. Qiao, *Appl. Phys. Lett.*, 2008, **93**, 152905.

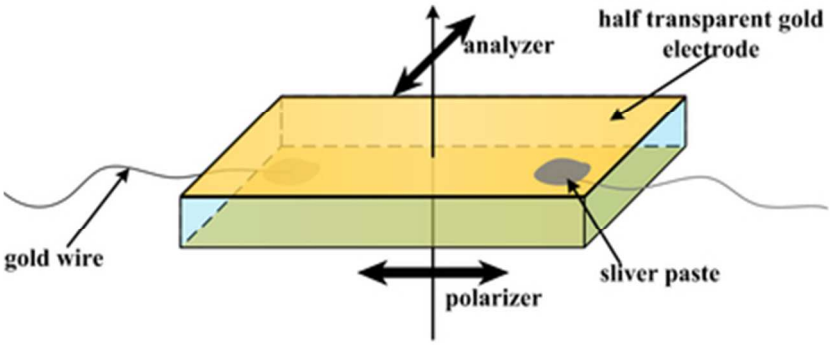

FIG. 1. (Color online) The illustration of the experimental configuration for observing domain structures under the polarizing microscope.
34x14mm (300 x 300 DPI)

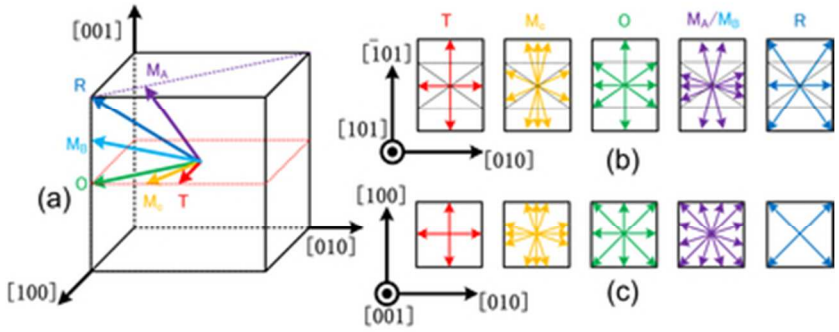

FIG. 2. (Color online) Schematics of (a)PS directions with respect to cubic unit cell for different FE phases and possible extinction positions of domains in (b) (101)pc and (c) (001)pc crystal plates.
35x14mm (300 x 300 DPI)

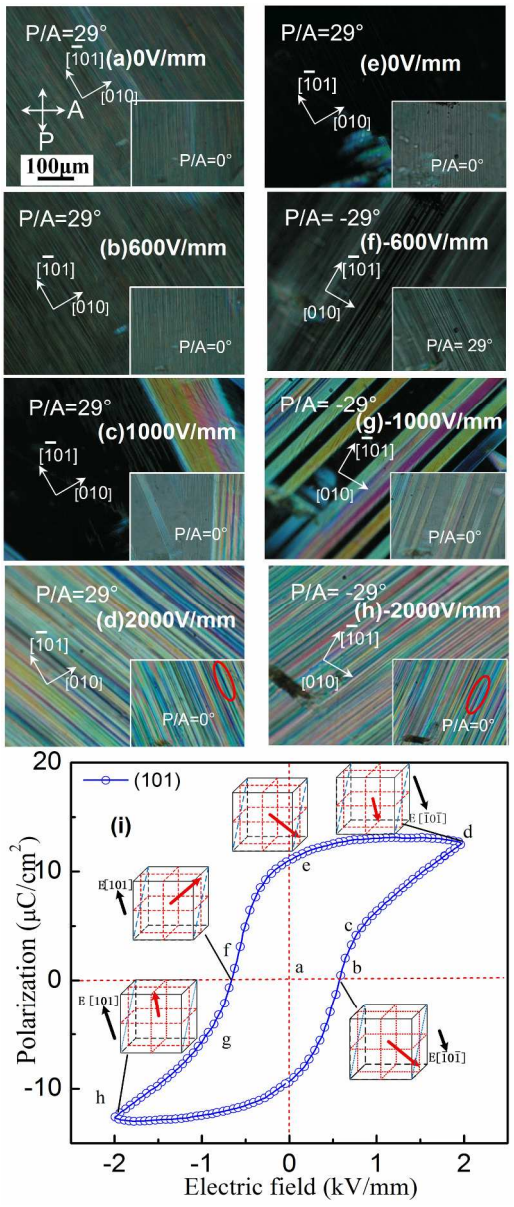

FIG. 3. (Color online) (a)- (h) are micrographs of (101)pc KNN25 crystals at different electric fields as stated. (i) illustrates the corresponding points of (a)-(h) in the hysteresis loop for (101)pc KNN25 crystals. The insets are the schematic configurations of PS states of the points indicated in the micrograph.
199x467mm (300 x 300 DPI)

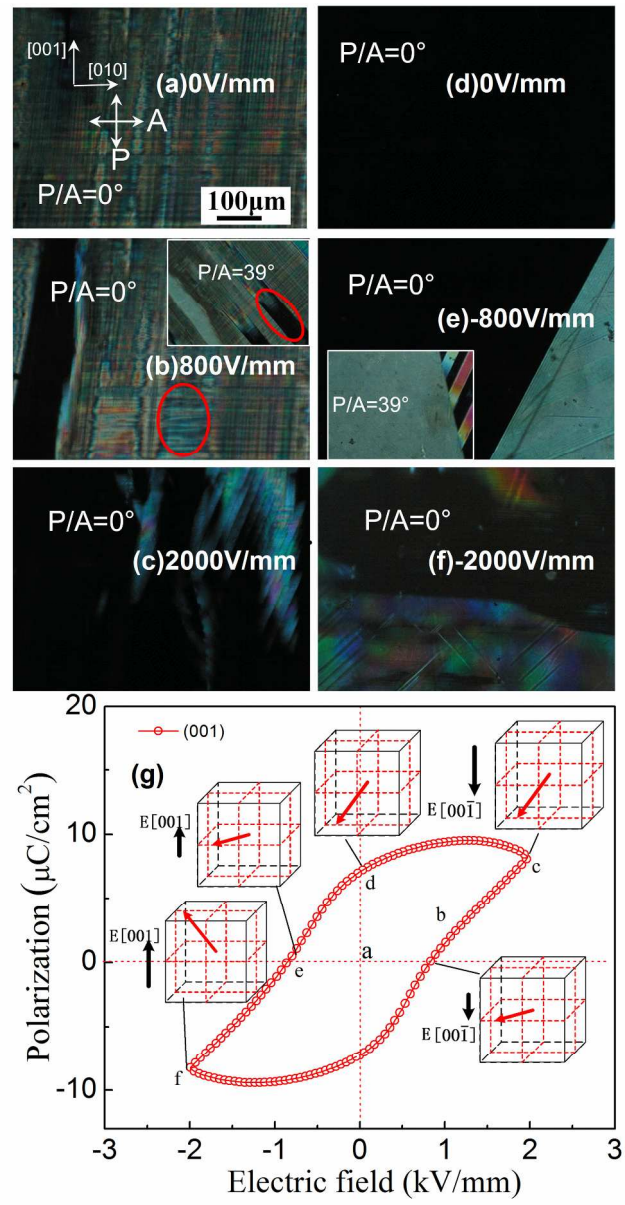

FIG. 4. (Color online) (a)- (f): micrographs of (001)pc KNN25 crystals at different electric fields as stated. (g) illustrates the corresponding points of (a)-(f) in the hysteresis loop for (001)pc KNN25 crystals. The insets are the schematic configurations of PS states of the points indicated in the micrograph.
161x305mm (300 x 300 DPI)

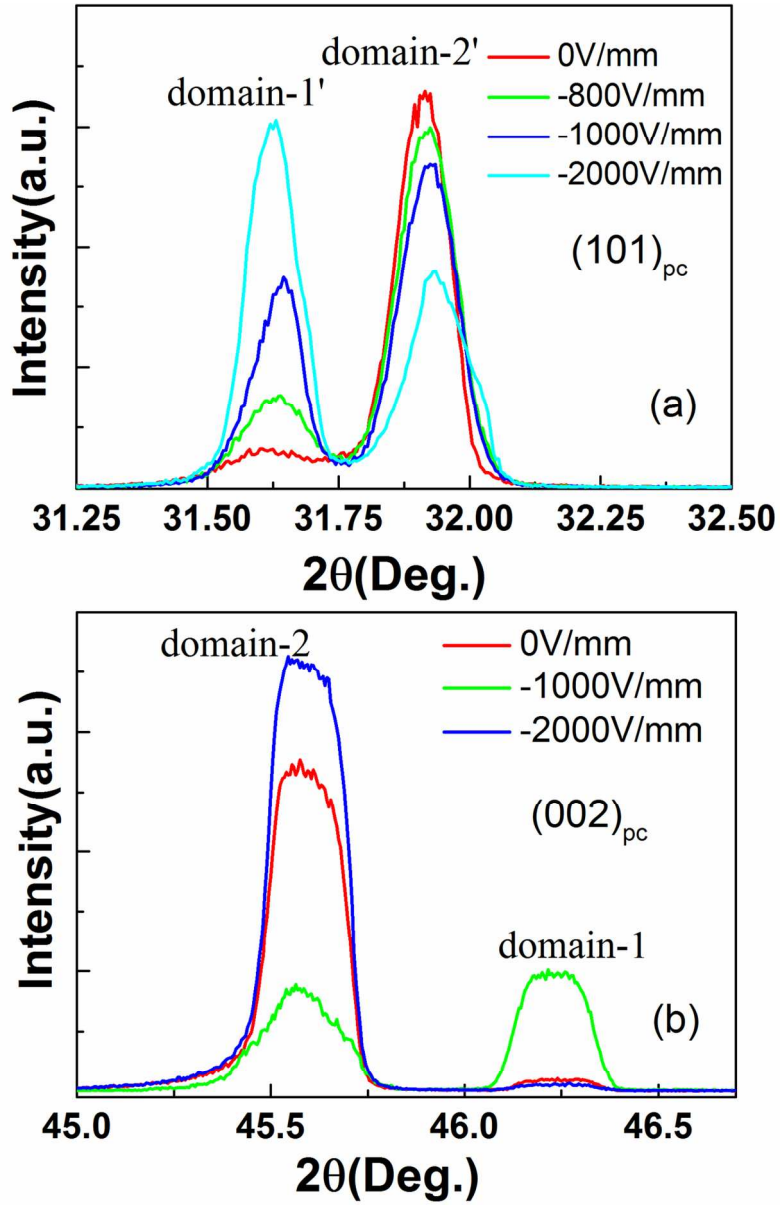

FIG. 5. (Color online) XRD patterns of (a) (101)pc and (b) (001)pc KNN25 crystals under electric field
107x165mm (300 x 300 DPI)